Materials Advances

PAPER

Check for updates

Comparative study of the thermal decomposition of ammonium nitrate in the presence of nanocrystalline copper ferrite

Pragnesh N. Dave [ID] * and Ruksana Sirach

This study aims to investigate the catalytic effects of nanocrystalline copper ferrite (CF) on the thermal decomposition of ammonium nitrate. We employed non-isothermal methods to determine the kinetic parameters of the thermal decomposition process for both pristine ammonium nitrate and ammonium nitrate/CF composition, based on thermal analysis data obtained at three different heating rates. Our findings indicate that CF remains stable within the temperature range of ammonium nitrate's decomposition, making it a viable catalyst for the decomposition of ammonium nitrate. The introduction of CF significantly reduced the activation energy required for the decomposition of ammonium nitrate. Notably, the ammonium nitrate/CF composition decomposed at a temperature 10 K lower than that of pure ammonium nitrate, with a remarkably low activation energy barrier of 81.3 ± 7.7 kJ mol^{-1}. These findings suggest that ammonium nitrate containing 2 wt% CF has the potential to serve as an improved energetic material, offering enhanced thermal performance compared to pure ammonium nitrate.

1. Introduction

Nanomaterials are a captivating class of materials, characterized by their small size dimensions, typically measuring <100 nm. Nanotechnology harnesses these materials at the nanoscale for various applications, including but not limited to medicinal applications, environmental remediation, catalysis, and energy storage.[1–7] Catalysis stands as one of the foremost applications of nanomaterials, with a particular emphasis on nanoscale materials based on transition metals. A catalyst is a chemical entity that expedites a chemical process by offering an alternative pathway for the reaction, remaining unaltered and unconsumed during the reaction. Materials such as ammonium nitrate and ammonium perchlorate (AP) decompose within a short period releasing large amounts of energy and gaseous products that can be used to propel objects. As a result, such materials are termed 'high energetic materials' and find extensive use in a range of applications, including missiles, firearms, mining, and rocket propulsion, among others. AP is currently among the most widely used energetic materials in solid propellants but its decomposition products are chlorine containing oxides which cause severe environmental problems.[8] Hence, ammonium nitrate is being explored as a potential replacement for AP-based propulsion formulations. Ammonium nitrate can be used in formulations such as powdered explosives,

ANFO, suspension explosives, emulsion explosives, and propellants, to name a few.[9–11] Owing to ammonium nitrate's chlorine-free combustion, low cost, and gas generation ability, it is used as a green oxidizer in various high-energetic applications.[12,13] Boukeciat *et al.*[14] investigated double base propellants, which consisted of 60% ammonium nitrate, 10% nitrocellulose, and 30% diethylene glycol dinitrate, to assess their thermal performance potential. The inclusion of ammonium nitrate not only lowered the activation energy of the propellant but also elevated the heat content during decomposition. Furthermore, certain ammonium nitrate-based co-crystals and composites show potential for serving as potential substitutes in a range of propulsion formulations due to their enhanced thermal performance, which can be further enhanced with the use of a catalyst.[15–18]

Ammonium nitrate is hygroscopic and often suffers from low burning and explosive performance.[9,19] It has been reported that the incorporation of a small amount of metallic alloys can improve the detonation of ammonium nitrate and its burning characteristics.[9,11] A previous study[19] suggested that the use of saccharides improves the burning rate of ammonium nitrate by decreasing the activation energy barrier. Ammonium nitrate crystals modified using carbohydrates exhibited a lower energy barrier of ~10 kJ mol^{-1} and a lower thermal decomposition temperature in the range of 5–9 °C.[19] Fe_2O_3 catalyzes the decomposition of ammonium nitrate by decreasing the activation energy, thereby increasing the ignition of ammonium nitrate.[20] Not all materials can improve the thermal

Department of Chemistry, Sardar Patel University, Vallabh Vidyanagar, 388 120, Gujarat, India. E-mail: pragnesh7@yahoo.com

decomposition characteristics of ammonium nitrate.[21,22] Alkaline materials like $CaCO_3$ have been reported to inhibit the decomposition of ammonium nitrate.[21,23] In a recent study, Kaniewski et al.[21] investigated the decomposition of various ammonium nitrate compositions. Ammonium nitrate was combined with additives like sulfate salts of NH_4^+, Mn^{2+}, Fe^{3+}, Cu^{2+}, Zn^{2+}, and Ca^{2+} and the decomposition of the resulting composition was studied. The diverse compositions manifest either single- or two-stage decomposition profiles. Notably, in the case of a 49 : 1 mixture of ammonium nitrate and $ZnSO_4$, the peak decomposition temperature of ammonium nitrate decreased from 284.3 ± 0.5 to 277.8 ± 3.4 °C. It is important to note that these additives interact with ammonium nitrate, indicating that it does not function as a catalyst. In yet another study, the authors documented that the presence of magnesium chloride led to the decomposition of ammonium nitrate with a maximum decomposition temperature of 268.8 ± 2.3 °C, while the presence of potassium chloride resulted in a reduction of the maximum decomposition temperature to 261.1 ± 2.3 °C, occurring within a broad temperature range.[24,25]

To balance the thermal stability and energetic performance of ammonium nitrate, various studies have been conducted to improve the thermal decomposition properties of ammonium nitrate. Previous studies have reported that the thermal decomposition of ammonium nitrate can be tailored by the addition of a catalyst or the formation of co-crystals with other highly energetic materials.[17,26–29] Burning rate is one of the most important parameters for the solid propellant performance. Vara et al.[26,27] documented that a decreased decomposition temperature of ammonium nitrate can directly influence the burning rate of ammonium nitrate-based propellants. Vara and Dave[26] studied bimetallic transition metal oxides based on Co, Cu, and Ni as a potential catalyst for the thermal decomposition of ammonium nitrate. The research revealed that CuZnO was capable of significantly reducing the activation energy of ammonium nitrate and achieved a reduction of up to 94 kJ mol^{-1}, resulting in an enhanced burning rate when compared to propellants based on pure ammonium nitrate. Sun et al.[12] reported that the presence of sulfuric acid or copper oxide contaminations in ammonium nitrate leads to faster decomposition. Although many studies have focused on improving the thermal decomposition performance of ammonium nitrate, it is still a developing field. Utilizing an appropriate catalyst can lead to a better thermal decomposition performance of ammonium nitrate.

The magnetic nature of ferrites has attracted a lot of attention in catalysis applications owing to ease of synthesis and separation after application. Ferrites have a general formula MFe_2O_4 and can be easily synthesized using methods like co-precipitation, combustion, sol–gel, hydrothermal, and thermal decomposition.[30] Moreover, M^{2+} cations like Co^{2+}, Cu^{2+}, Zn^{2+}, and Mg^{2+} can act as Lewis acid sites in the elimination of NH_3 during the thermal decomposition of ammonium nitrate.[31] Therefore, the authors have focused on the utilization of copper ferrite ($CuFe_2O_4$ or CF) as a potential catalyst to decrease the activation energy of thermolysis of ammonium nitrate.

In the present work, the authors have synthesized nanocrystalline CF catalysts and studied their structural parameters using X-ray diffraction (XRD) and Fourier transform infrared (FTIR) spectroscopy. The comparative decomposition of ammonium nitrate and ammonium nitrate with 2% (by mass) CF additive was investigated using thermal analysis techniques. The catalytic activity of CF on the decomposition of ammonium nitrate was investigated using thermal data at three heating rates using iso-conversion methods.

2. Experimental

2.1. Preparation of CF and ammonium nitrate/CF

All chemicals were of reagent grade (supplied by SRL PVT. Ltd, India) and used as received without any modifications.

The nanocrystalline CF was synthesized by the co-precipitation method. A total of 150 mL of 0.2 M copper nitrate salt ($Co(NO_3)_2 \cdot 6H_2O$; 99%) solution was mixed with 150 mL of 0.4 M ferric nitrate salt ($Fe(NO_3)_3 \cdot 9H_2O$; 98%) solution. This solution was subjected to continuous magnetic stirring. Subsequently, 2 M sodium hydroxide (NaOH; 99%) was added to the metal nitrate mixture under vigorous stirring until the solution attained a pH of ~ 11–12. The resulting precipitates were filtered and washed with warm water to eliminate impurities. Finally, CF was obtained by calcinating the dried CF powder in an oven at 500 °C for 5 h.

Further, 0.002 g of CF and 0.098 g of ammonium nitrate (ammonium nitrate/CF) were mixed using a mortar-pestle. The thermal decomposition characteristics of this ammonium nitrate/CF mixture were investigated using TG-DSC analysis and compared to those of pure ammonium nitrate.

2.2 Characterization

The structural parameters of CF were investigated using the powder XRD (Rigaku Ultima IV Diffractometer; Cu Kα; $\lambda = 0.15406$ nm) technique and FTIR spectroscopy (FTIR-8400S, Shimadzu spectrophotometer). The morphology of CF was investigated using scanning electron microscopy (FE-SEM; Nova nano FEG-SEM 450). The thermal decomposition and kinetic parameters of ammonium nitrate, both in the presence and absence of the CF additive, were thoroughly investigated using simultaneous thermo-gravimetry (TG)/differential scanning calorimetry (DSC) analysis (PerkinElmer STA 8000, alumina pan, N_2 atmosphere). The TG-DSC analysis was performed at three distinct heating rates (5, 10, and 15 K min^{-1}) within the temperature range 303–673 K.

2.3. Kinetic analysis

Kinetic analysis is crucial for gaining insights into the kinetic triplet, which comprises the activation energy, pre-exponential factor, and the reaction mechanism of a material. To assess the thermal decomposition kinetics of materials, model-free and model-fitting isoconversion methods are commonly employed. However, it is important to note that relying on a single heating rate for evaluation can introduce inaccuracies. Therefore, it is recommended to utilize a minimum of three distinct heating rates to accurately determine the various kinetic parameters

associated with the decomposition process.[32–34] In a non-isothermal, isoconversion method, at a constant conversion (α), the reaction rate ($k(T)$) is affected by the temperature (eqn (1)):[14]

$$\frac{d\alpha}{dT} = k(T)f(\alpha) \qquad (1)$$

where $f(\alpha)$ is the differential model.

Consequently, we investigated the kinetics of the thermal decomposition of ammonium nitrate employing non-isothermal methods, like the Kissinger–Akahira–Sunose (KAS) (eqn (2)), Flynn–Wall–Ozawa (FWO) (eqn (3)), and Starink methods (eqn (4)):

$$\ln\left(\frac{\beta}{T^2}\right) = \ln\left(\frac{AR}{g(\alpha)E}\right) - \frac{E}{RT} \qquad (2)$$

$$\ln\beta = \ln\left(\frac{0.0048AE}{g(\alpha)R}\right) - 1.0516\frac{E}{RT} \qquad (3)$$

$$\ln\left(\frac{\beta}{T^{1.92}}\right) = \ln\left(\frac{AR^{0.92}}{E^{0.92}}\right) - 0.312 - 1.0008\frac{E}{RT} \qquad (4)$$

where A, E, β, T, and R represent the pre-exponential factor, activation energy, heating rate, peak temperature, and the universal gas constant, respectively. $g(\alpha)$ is the integral reaction model. The plot of $\ln\beta$, $\ln\beta/T^2$, and $\ln\beta/T^{1.92}$ against $1000/T$ was used to determine the kinetic parameters. The A and E values for the decomposition of ammonium nitrate, in the presence and absence of the CF catalyst, were determined from the interception and slope of these plots, respectively.

3. Results and discussions

3.1 Characterization

FT-IR analysis provides insights into the vibrational behaviour of atoms on the surface of nanocrystalline CF. The FTIR spectrum (see Fig. 1) confirmed the formation of spinel ferrite, $CuFe_2O_4$. Notably, the peaks observed within the 800–500 cm^{-1} range are characteristic peaks of ferrites. The peak at 592 cm^{-1} corresponds to the stretching vibration of Fe^{3+}–O in the tetrahedral site, whereas the peak at 547 cm^{-1} is attributed to the vibration of M^{2+}–O in the octahedral site. It is worth noting that for spinel ferrites like $MgFe_2O_4$ and $NiFe_2O_4$, these peaks are typically observed at 460 and $\sim$570 cm^{-1}.[30] The peak observed at 3500 cm^{-1} corresponds to the hydroxyl groups located on the surface of CF. The band in the range of 1600–1500 cm^{-1} is associated with the bending vibrations of the absorbed water molecules. Additionally, the bands within the 900–800 and 1200–950 cm^{-1} regions are likely attributed to the residual FeOOH.[35]

The XRD patterns of CF, as depicted in Fig. 2, were compared and matched with Ref. no. 00-025-0283. Notably, CF exhibits diffraction peaks within the angular range of $10° < 2\theta < 70°$, indicating its cubic structure with angles $\alpha = \beta = \gamma = 90°$. The specific CF diffraction peaks occurring at 2θ angles of 18.5°, 29.5°, 35.5°, 38.8°, 41.3°, 57.1°, and 63.9° correspond to (111), (220), (311), (222), (400), (511), and (440) lattice planes, respectively. The average crystalline size[36,37] of CF calculated using the
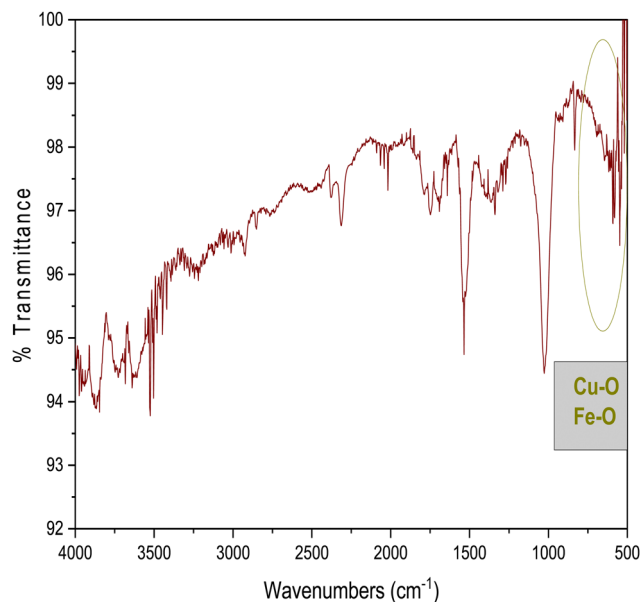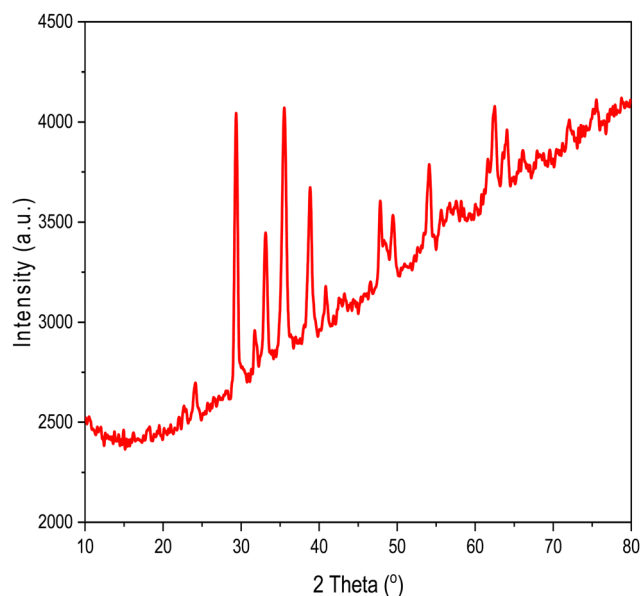

Fig. 1 FITR spectrum of copper ferrite (CF).

Fig. 2 XRD patterns of copper ferrite (CF).

Scherrer equation was 18 nm, confirming the formation of nanocrystalline CF. Further, structural parameters of CF were derived from the (311) lattice plane using eqn (5)–(8):

$$a = d(h^2 + k^2 + l^2)^{1/2} \qquad (5)$$

$$\rho = \frac{8M}{N_A V} \qquad (6)$$

$$\varepsilon = \frac{\beta\cos\theta}{4} \qquad (7)$$
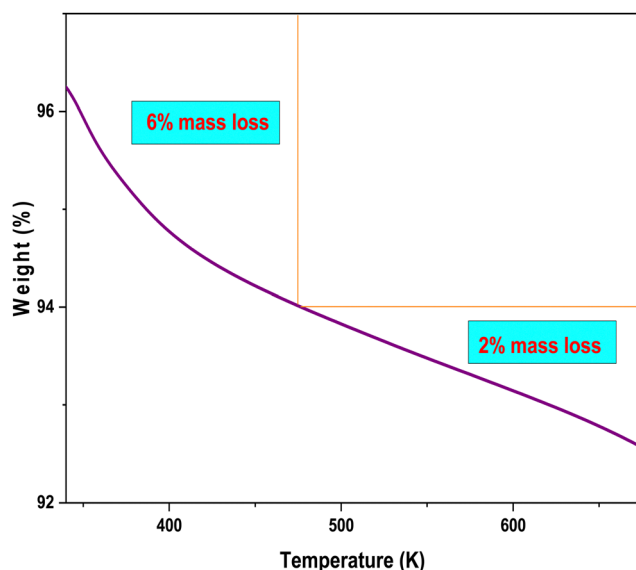
$$\delta = \frac{1}{D^2} \qquad (8)$$

Table 1 Parameters derived from the XRD diffraction peak belonging to the 311 plane

Cell constant (nm)	Crystalline size (nm)	Microstrain	X-Ray density (g cm^{-3})	Dislocation density (lines m^{-2})
0.837	18	0.00302	5.41	3.09×10^{15}

where θ, a, d, ρ, M, N_A, V, ε, β, δ, and D represent Bragg's angle ($2\theta/2$), lattice constant ($a = b = c$), lattice spacing corresponding to the 311 plane, X-ray density, molar mass, Avogadro's constant, cell volume ($V = a^3$), microstrain, full width at half-maxima corresponding to the 311 plane, dislocation density and crystalline size, respectively. The values of various parameters are reported in Table 1.

Kombaiah *et al.*[38] previously published lattice parameters of 0.836 nm for copper ferrite with a crystalline size of 62 nm, and 0.837 nm for copper ferrite with a crystalline size of 25 nm. The current results align more closely with the values reported by Kombaiah *et al.*[38] However, it is worth noting that there is a significant variation in microstrain values. The microstrain value in our study is in closer agreement with the findings of Samson *et al.*,[39] where the authors reported a microstrain value of 0.00359 for a 21.4 nm size CF. These variations in the microstrain value suggest that the distribution of atomic-level strain within the CF varies along the scattering vector.

The TG thermogram (Fig. 3) indicates that CF remains stable within the studied temperature range of ammonium nitrate (*i.e.*, 303–673 K). The initial mass loss, occurring up to 473 K, can be attributed to the loss of water[40–43] adsorbed on the surface of CF, which likely evaporates and results in a 6% mass loss. In the temperature range of 473–673 K, only a minimal 2% mass loss is observed. This finding underscores the thermal stability of CF, suggesting that it will not cause major fluctuations in the TG curve of ammonium nitrate when used as a catalyst. The 2% mass loss in this temperature range is attributed to the vaporization of hydroxyl groups from the surface of CF.

SEM images (Fig. 4) provide insights into the morphology of CF. The nanoparticles exhibited irregular shapes, displaying a variety of forms, including deformed shapes such as hexagonal, spherical, and cubic shapes. Notably, the SEM image of CF revealed the coexistence of micron-scale particles alongside the nanoscale ones. This phenomenon may be attributed to the aggregation of nanocrystalline CF particles, leading to the formation of larger micron-sized particles. However, it is worth noting that a few isolated micron-size particles may have originated due to the inherent tendency of the co-precipitation method to yield a broad range of particle sizes.

3.2. Thermal decomposition and kinetics

In the DSC curve of pure ammonium nitrate (Fig. 5b), five endothermic curves were observed. The curve observed between the temperature range of 313–333 K is attributed to the polymorphic transition of ammonium nitrate from the tetragonal to orthorhombic form. The endotherm in the temperature range of 353–373 K corresponds to the orthorhombic-to-orthorhombic phase transition of ammonium nitrate because of the presence of moisture. The peak between 393 and 413 K is attributed to the

Fig. 3 TG curve of copper ferrite (CF).
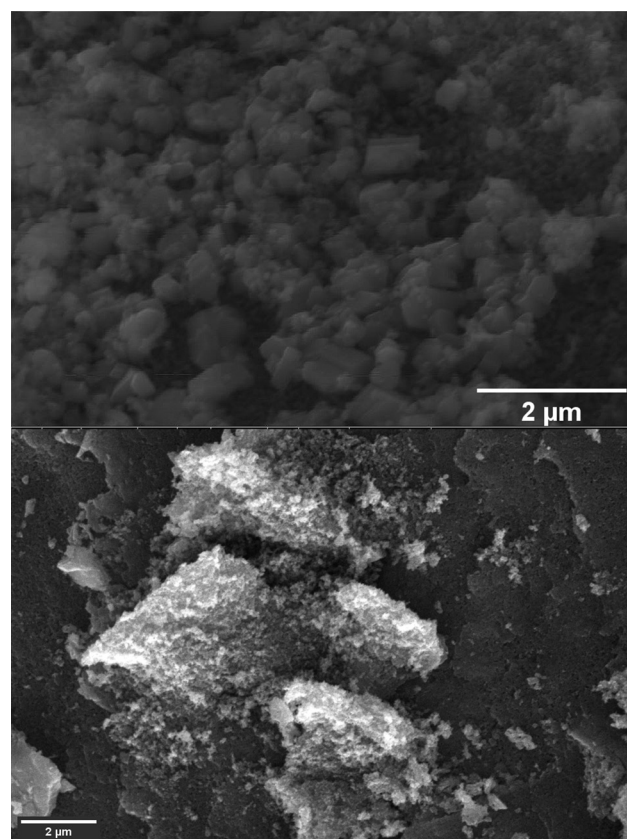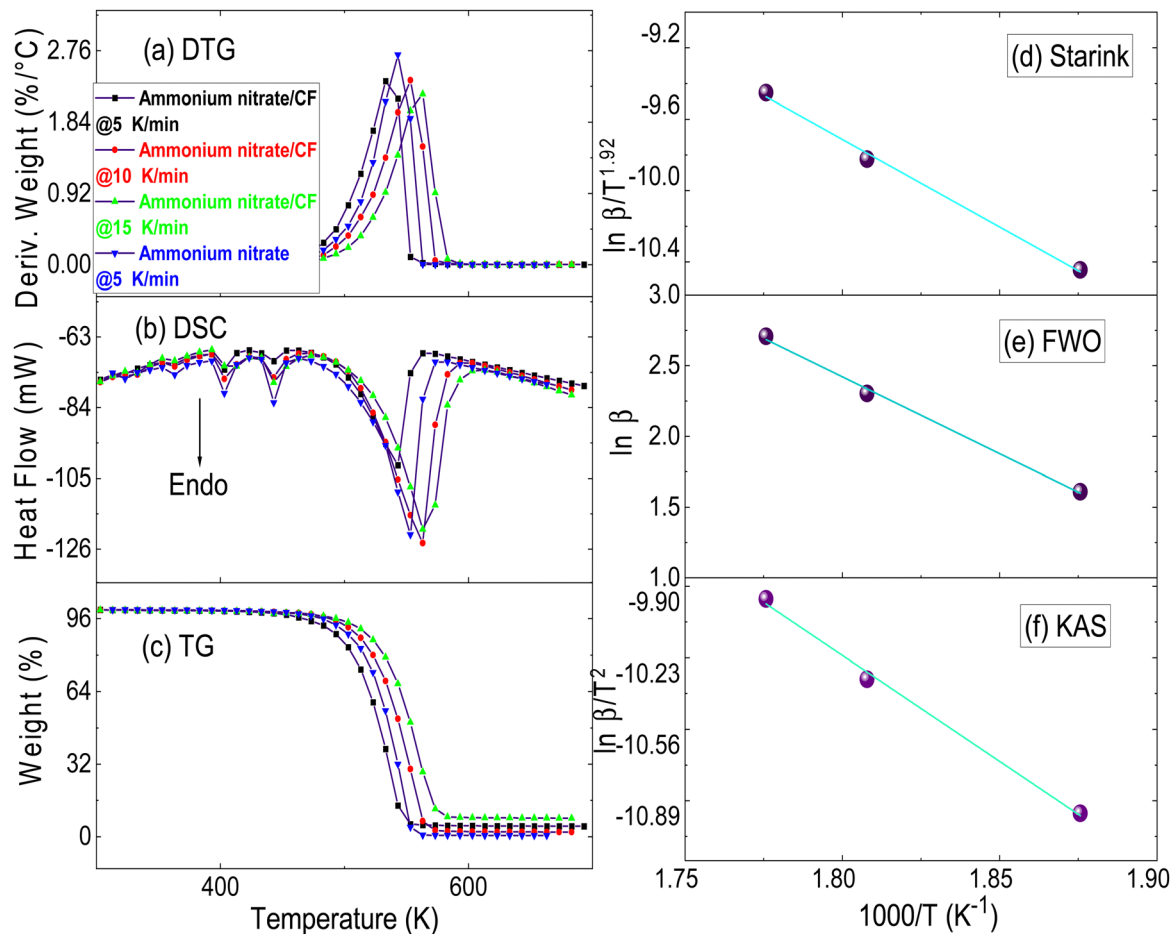

Fig. 4 SEM images of copper ferrite (CF).

Fig. 5 (a) DTG, (b) DSC, and (c) TG curve of pure ammonium nitrate (β = 5 K min^{-1}) and ammonium nitrate/CF (5, 10, and 15 K min^{-1}). Starink (d), FWO (e), and KAS (f) plots of ammonium nitrate/CF.

phase transition of ammonium nitrate from the orthorhombic to the cubic phase. Subsequently, melting of ammonium nitrate at 443 K resulted in another endothermic curve.[44,45] Ammonium nitrate decomposes after melting at a maximum peak temperature of 543 K, suggesting that the decomposition of ammonium nitrate occurred in a liquid state. The mass loss (Fig. 5a and c) during the phase transition of ammonium nitrate up to 443 K was only 0.9% which could be attributed to the loss of moisture during heating. The decomposition of ammonium nitrate starts quickly after being in the liquid state with a sudden and substantial mass loss of >99% at 543 K. The decomposition of ammonium nitrate occurs between 453 and 563 K. It is speculated that the initiation of ammonium nitrate decomposition involves an endothermic proton transfer process. In this process, ammonium nitrate is decomposed into NH_3 and HNO_3, which subsequently undergo oxidation to produce various gaseous products, such as H_2O and N_2O, resulting in a sudden mass loss of >99%. Catalysts like CF can exert an influence on the decomposition of ammonium nitrate by facilitating the breakdown of NH_4NO_3 into NH_3 and HNO_3, while also aiding in the oxidation of these intermediates.

When 2% CF is introduced, the phase transitions of ammonium nitrate/CF are observed within the temperature ranges of 313–333, 353–373, and 393–413 K. The melting of ammonium

nitrate/CF occurs at 443 K (Fig. 5b). Incorporation of CF does not alter the phase transition peaks and the melting point of ammonium nitrate; however, the decomposition of ammonium nitrate is impacted, which occurs at a lower temperature in the presence of CF, signifying the CF's role in facilitating the decomposition process of ammonium nitrate. In previous studies,[21,24,25] it was reported that the incorporation of additives like metal ion salts can alter all curves, including the phase transition, melting temperatures and decomposition temperatures of ammonium nitrate. In our study, we observed that CF exclusively affects the decomposition peak of ammonium nitrate. The decomposition of ammonium nitrate/CF commences at 443 K (Table 2), which is 10 K lower than the initial decomposition temperature of ammonium nitrate. Within the temperature range of 443–553 K, there is a significant mass loss of ammonium nitrate/CF, exceeding 97%. The maximum mass loss of ammonium nitrate/CF occurs at 533 K, which is 10 K lower than pure ammonium nitrate. The difference between the onset (initial) temperature and peak or maximum temperature for both ammonium nitrate/CF and pure ammonium nitrate remains the same. This suggests that the decomposition process likely follows a similar pathway in both cases. CF primarily serves to lower the temperature at

Table 2 Comparison of the thermal decomposition temperature and activation energy of ammonium nitrate in the presence of CF catalyst

Catalyst	Temperature (K)			E^a (kJ mol^{-1})	Nature of the decomposition peak	Mass loss (%)
	Onset (T_o)	Peak (T_p)	$\Delta T = T_p - T_o$			
Ammonium nitrate	453	543	90	155.8 ± 2.0	Endothermic	99.3
Ammonium nitrate/CF	443	533	90	81.3 ± 7.7	Endothermic	97.3

^{a} The KAS method.

which the ammonium nitrate decomposition occurs but does not alter the fundamental decomposition pathway. The same can be concluded from the DSC curve of ammonium nitrate and ammonium nitrate/CF at a 5 K min^{-1} heating rate. The activation energy calculations confirm that CF lowers the activation energy of ammonium nitrate and makes it more feasible than pure ammonium nitrate. The peak temperature of DTG curves of ammonium nitrate/CF at 5, 10, and 15 K min^{-1} was used to plot Starink, FWO, and KAS plots (Fig. 5(d–f)). The coefficient of determination (R^2) for all plots was >0.99 suggesting a good statistical relation. The activation energies determined for ammonium nitrate were found to be 156.2 ± 2.0, 155.8 ± 2.0, and 164.5 ± 2.0 kJ mol^{-1} by using the Starink, KAS, and FWO methods, respectively. The activation energy of ammonium nitrate/CF was largely decreased. The activation energies determined for the ammonium nitrate/CF system were found to be 81.6 ± 7.7, 81.3 ± 7.7, and 85.9 ± 3.2 kJ mol^{-1} when employing the Starink, KAS, and FWO methods, respectively. The activation energy of ammonium nitrate was ~1.92 times higher than compared to ammonium nitrate/CF. The pre-exponential factor (ln A) for the decomposition process of ammonium nitrate was found to be 12.3 ± 1, 12.0 ± 1, and 18.4 ± 1 min^{-1} by using the Starink, KAS, and FWO methods, respectively. Similarly, for the ammonium nitrate/CF system, the ln A values were found to be 5.23 ± 1.67, 9.67 ± 1.68, and 15.50 ± 1.67 min^{-1} using the same methods. The comparatively lower ln A values for the ammonium nitrate/CF decomposition process imply a faster decomposition rate than ammonium nitrate. From the kinetic data and thermal data, it can be concluded that CF not only decreases the decomposition temperature of ammonium nitrate but also increases the thermal decomposition of ammonium nitrate by lowering the activation energy barrier.

The thermodynamic parameters such as enthalpy change (ΔH), free energy change (ΔG), and entropy change (ΔS) were calculated from eqn (9)–(11):

$$\Delta H = E - RT \quad (9)$$

$$\Delta S = R[\ln A - \ln(k_B T/h)] \quad (10)$$

$$\Delta G = \Delta H - T\Delta S \quad (11)$$

where k_B is the Boltzmann constant and h is the Planck constant.

The enthalpy change of ammonium nitrate was decreased from 151.3 to 76.9 ± 7.7 kJ mol^{-1}, the entropy change was decreased from -0.148 ± 0.008 to -0.169 ± 0.014 kJ mol^{-1}, and the free energy change was decreased from 231.6 ± 2.5 to 167.2 ± 15.2 kJ mol^{-1}, upon addition of 2% CF. The decreased values of free energy and enthalpy suggest a thermodynamically favorable decomposition of ammonium nitrate/CF than ammonium nitrate.

In the presence of additives, ammonium nitrate can have either endothermic or exothermic curves depending on the decomposition pathways. It was assumed that the additives that give an exothermic curve of ammonium nitrate usually facilitate a different decomposition pathway for ammonium nitrate.[46] It was reported that the generation of NH_3 and HNO_3 as decomposition products leads to an endothermic curve, while the formation of N_2O and H_2O leads to an exothermic curve.[45,46] The intermediates produced during the decomposition of ammonium nitrate can get adsorbed on the surface of the catalyst and can be further oxidized (see Fig. 6).
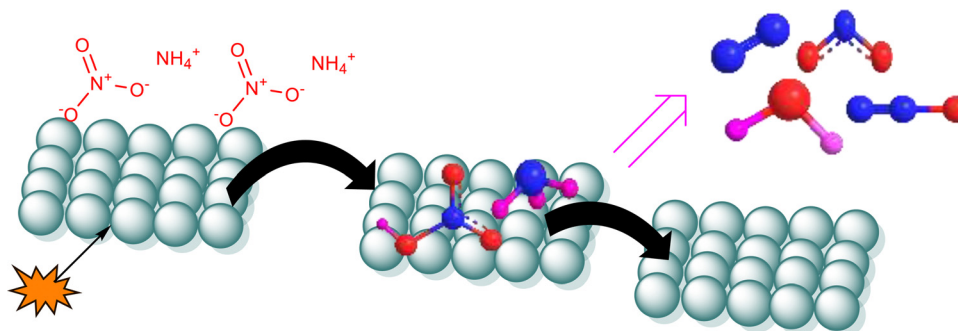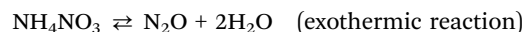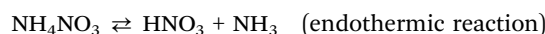
$$NH_4NO_3 \rightleftarrows HNO_3 + NH_3 \quad \text{(endothermic reaction)}$$

$$NH_4NO_3 \rightleftarrows N_2O + 2H_2O \quad \text{(exothermic reaction)}$$

Fig. 6 Schematic representation of the thermal decomposition mechanism of ammonium nitrate in the presence of CF.

Table 3 Comparison of peak temperatures and activation energies of ammonium nitrate in the presence of various catalysts

Composition	Peak temperature (K)	Activation energy (kJ mol^{-1})	Nature of the peak	Ref.
Ammonium nitrate + 2 wt% CF	533	81.3 ± 7.7	Endothermic	Present work
Ammonium nitrate + 1 wt% CuZnO	552	97.7	Exothermic	26
Ammonium nitrate + 1 wt% CoMn ferrite	544	98.0	Exothermic	27

CF significantly reduces the activation energy of ammonium nitrate, resulting in the final decomposition of ammonium nitrate/CF occurring at a peak temperature of 533 K, characterized by a notably reduced activation energy barrier of only 81.3 ± 7.7 kJ mol^{-1}. The obtained result was better than those reported previously for other catalysts; some of them are given in Table 3 for comparison.[26,27,31] In the presence of CuZnO and CoMn ferrite, the decomposition curve of ammonium nitrate was exothermic indicating different decomposition mechanism pathways of ammonium nitrate. However, CF does not alter the decomposition products of ammonium nitrate but only decreases the energy barrier. Hence, ammonium nitrate/CF can be used instead of ammonium nitrate for high energetic applications.

4. Conclusions

In the present work, nanocrystalline (18 nm) CF was synthesized and studied as a catalyst to improve the thermal decomposition of ammonium nitrate using non-isothermal methods. The findings of the work suggested that incorporating only a small amount of CF (2% by mass) into ammonium nitrate can decrease the peak decomposition temperature of ammonium nitrate by 10 K without drastically impacting the transition temperature of ammonium nitrate. During the decomposition of ammonium nitrate, CF is quite stable (8% mass loss up to a temperature of 673 K), and hence, does not decompose during the decomposition of ammonium nitrate. The addition of CF (2% by mass) was able to decrease the activation energy of ammonium nitrate to 81.3 ± 7.7 kJ mol^{-1}, with a natural logarithm (ln) of the pre-exponential factor (A) at 9.67 ± 1.68 min^{-1}. The findings of the present work suggest that due to the lower activation energy, ammonium nitrate/CF decomposes more rapidly at a lower temperature compared to pure ammonium nitrate. Furthermore, the thermodynamic analysis indicated that the decomposition of ammonium nitrate/CF was more thermodynamically favorable than that of pure ammonium nitrate. These findings hold promise for the application of ferrites containing transition metal ions as catalysts to facilitate the thermal breakdown of ammonium nitrate, making it a potential high-energy material for use in propellant formulations.

Author contributions

PND contributed to data validation, supervision, providing necessary resources, and finalizing the draft manuscript. RS

contributed to the methodology, formal analysis, data curation, and writing the original draft.

Data availability

Data are available upon request.

Conflicts of interest

Authors declare no competing financial and/or non-financial interests in relation to the work described.

References

1 F. Deng, Y. Wu, W. Tang, S. Song, Z. Wen, M. Kotobuki, L. Lu, J. Yao, N. Hu and J. Molenda, *Solid State Ionics*, 2019, **342**, 115063.

2 M. Laayati, A. Abdelkader Mekkaoui, L. Fkhar, M. A. Ali, H. Anane, L. Bahsis, L. E. Firdoussi and S. E. Houssame, *RSC Adv.*, 2022, **12**, 11139–11154.

3 F. Ganjali, A. Kashtiaray, S. Zarei-Shokat, R. Taheri-Ledari and A. Maleki, *Nanoscale Adv.*, 2022, **4**, 1263–1307.

4 M. Verma, M. Mitan, H. Kim and D. Vaya, *J. Phys. Chem. Solids*, 2021, **155**, 110125.

5 P. A. Ajibade and A. E. Oluwalana, *Nanomaterials*, 2021, **11**, 2000.

6 I. Hussain, T. Hussain, S. Yang, Y. Chen, J. Zhou, X. Ma, N. Abbas, C. Lamiel and K. Zhang, *Chem. Eng. J.*, 2021, **413**, 127570.

7 M. Ebadi, K. Buskaran, S. Bullo, M. Z. Hussein, S. Fakurazi and G. Pastorin, *Alexandria Eng. J.*, 2021, **60**, 733–747.

8 Y. Wang, X. Song and F. Li, *ACS Omega*, 2019, **4**, 214–225.

9 J. Paszula, A. Maranda, B. Kukfisz and P. Putko, *Energies*, 2022, **15**, 8803.

10 S. Touidjine, M. Karim Boulkadid, D. Trache, S. Belkhiri, A. Mezroua, M. Islam Aleg and A. Belkebiche, *Def. Technol.*, 2022, **18**, 2023–2033.

11 M. Kohga and S. Togo, *Combust. Sci. Technol.*, 2020, **192**, 1668–1681.

12 Q. Sun, L. Jiang, H. Cao, J. Sun and G. Liu, *Appl. Therm. Eng.*, 2020, **181**, 116044.

13 T. Rotariu, B.-G. Pulpea, F.-M. Dîrloman, A. Diacon, E. Rusen, G. Toader, N.-D. Zvîncu, T.-V. Iordache and R. H. Botiş, *Materials*, 2022, **15**, 8960.

14 H. Boukeciat, A. F. Tarchoun, D. Trache, A. Abdelaziz, R. Ahmed Hamada, A. Bouhantala, C. Bousstila, S. Hanafi, M. Dourari and T. M. Klapötke, *Materials*, 2022, **15**, 8138.

15 H. Boukeciat, A. F. Tarchoun, D. Trache, A. Abdelaziz, R. Meziani and T. M. Klapötke, *Polymers*, 2023, **15**, 1799.

16 A. Abdelaziz, A. F. Tarchoun, H. Boukeciat and D. Trache, *Energies*, 2022, **15**, 6722.

17 S. Hanafi, D. Trache, R. Meziani, H. Boukeciat, A. Abdelaziz, A. F. Tarchoun and A. Mezroua, *Thermochim. Acta*, 2022, **717**, 179324.

18 S. Hanafi, D. Trache, R. Meziani, H. Boukeciat, A. F. Tarchoun, A. Abdelaziz and A. Mezroua, *FirePhysChem*, 2022, **2**, 315–322.

19 I. Oluwoye, M. Altarawneh, J. Gore and B. Z. Dlugogorski, *Combust. Flame*, 2020, **213**, 132–139.

20 I. Oluwoye, S. Mosallanejad, G. Soubans, M. Altarawneh, J. Gore and B. Z. Dlugogorski, *Fire Saf. J.*, 2021, **120**, 103063.

21 M. Kaniewski, M. Biegun and J. Hoffmann, *J. Therm. Anal. Calorim.*, 2023, DOI: 10.1007/s10973-023-12328-5.

22 K. G. Gorbovskiy, A. I. Kazakov, A. M. Norov and A. I. Mikhaylichenko, *Theor. Found. Chem. Eng.*, 2021, **55**, 742–747.

23 E. Menicacci, P. Rotureau, G. Fayet and C. Adamo, *ACS Omega*, 2020, **5**, 5034–5040.

24 J. Hoffmann, M. Kaniewski, D. Nieweś and K. Hoffmann, *Pol. J. Chem. Technol.*, 2020, **22**, 1–8.

25 M. Kaniewski, K. Hoffmann and J. Hoffmann, *Thermochim. Acta*, 2019, **678**, 178313.

26 J. A. Vara and P. N. Dave, *Chem. Phys. Lett.*, 2019, **730**, 600–607.

27 J. A. Vara, P. N. Dave and S. Chaturvedi, *Part. Sci. Technol.*, 2021, **39**, 1–9.

28 S. Hanafi, D. Trache, R. Meziani, H. Boukciat, A. Mezroua, A. F. Tarchoun and M. Derradji, *Chem. Eng. J.*, 2021, **417**, 128010.

29 S. Hanafi, D. Trache, A. Mezroua, H. Boukeciat, R. Meziani, A. Fouzi Tarchoun and A. Abdelaziz, *RSC Adv.*, 2021, **11**, 35287–35299.

30 E. M. Masoud, A. A. El-Bellihi, W. A. Bayoumy and A. S. Abdallah, *Adv. Polym. Technol.*, 2018, **37**, 3711–3722.

31 A. Cabrera, C. R. Torres, L. Juncal, M. Meyer and S. Stewart, *Appl. Energy Combust. Sci.*, 2021, **6**, 100026.

32 D. Trache, *Carbohydr. Polym.*, 2016, **151**, 535–537.

33 D. Trache, A. Abdelaziz and B. Siouani, *J. Therm. Anal. Calorim.*, 2017, **128**, 335–348.

34 S. Vyazovkin, A. K. Burnham, J. M. Criado, L. A. Pérez-Maqueda, C. Popescu and N. Sbirrazzuoli, *Thermochim. Acta*, 2011, **520**, 1–19.

35 S. Pavithradevi, N. Suriyanarayanan and T. Boobalan, *J. Magn. Magn. Mater.*, 2017, **426**, 137–143.

36 E. M. Masoud, *Polym. Test.*, 2016, **56**, 65–73.

37 E. M. Masoud, M. E. Hassan, S. E. Wahdaan, S. R. Elsayed and S. A. Elsayed, *Polym. Test.*, 2016, **56**, 277–286.

38 K. Kombaiah, J. J. Vijaya, L. J. Kennedy, M. Bououdina and B. Al-Najar, *J. Phys. Chem. Solids*, 2018, **115**, 162–171.

39 V. A. F. Samson, S. B. Bernadsha, M. Mahendiran, K. L. Lawrence, J. Madhavan, M. V. A. Raj and S. Prathap, *J. Mater. Sci.: Mater. Electron.*, 2020, **31**, 6574–6585.

40 E. M. Masoud, *Ionics*, 2019, **25**, 2645–2656.

41 E. M. Masoud, A.-A. El-Bellihi, W. A. Bayoumy and E. A. Mohamed, *J. Mol. Liq.*, 2018, **260**, 237–244.

42 M. Khairy, E. M. Kamar, M. Yehia and E. M. Masoud, *Biointerface Res Appl Chem*, 2021, **12**, 893–909.

43 E. M. Masoud, A. I. Abdelsamea, M. N. Elsabagh, S. L. Abdelaziz and A. M. Abbas, *J. Inorg. Organomet. Polym. Mater.*, 2023, **33**, 1983–1999.

44 I. Dellien, *Thermochim. Acta*, 1982, **55**, 181–191.

45 S. Chaturvedi and P. N. Dave, *J. Energ. Mater.*, 2013, **31**, 1–26.

46 V. Babrauskas and D. Leggett, *Fire Mater.*, 2020, **44**, 250–268.